Journal of Polymers and the Environment
https://doi.org/10.1007/s10924-023-03044-0

ORIGINAL PAPER

Bioinks Functionalized with Natural Extracts for 3D Printing

Izaskun Larraza[1] · Arantzazu Santamaria-Echart[2,3] · Isabel Fernandes[2] · Filomena Barreiro[2,3] · Aitor Arbelaiz[1] · Arantxa Eceiza[1]

Accepted: 24 August 2023

Abstract
In the search of materials valid for direct ink writing (DIW) 3D printing and with special interest for the biomedical and pharmaceutical applications, the development of bioactive inks for DIW is of great interest. For that purpose, in this work bioactive waterborne polyurethane–urea inks were prepared by addition of natural extracts (logwood, chestnut, and alder buckthorn) and cellulose nanofibers (CNF). The rheological behavior of the inks proved to be strongly dependent on the extract type and content, and the addition route used. Inks prepared by ex-situ incorporation of the extracts showed a strong gel-like behavior, as did inks prepared with chestnut and alder buckthorn extracts, which, in turn, hindered a continuous flow during the printing process, resulting in 3D printed parts with poor shape fidelity. On the other hand, inks prepared in-situ and with logwood extract showed more facility to flow and higher homogeneity, which translated in better printability and better shape fidelity, further enhanced for CNF containing inks. 3D printed composites showed reinforced mechanical behavior, as well as in materials with enhanced antibacterial behavior. Overall, the possibility to successfully prepare bioactive inks valid for 3D printing was proven.

Keywords Waterborne polyurethane–urea · 3D printing · Natural extracts · Bioactive inks · Antimicrobial scaffolds

1. Introduction

In recent years, additive manufacturing technologies, such as 3D printing, are experiencing a massive growth in interest and their use for biomedical and pharmaceutical applications is constantly increasing [1]. Among the various bioprinting technologies used in these fields, liquid extrusion-based or DIW 3D printing is one of the most popular techniques, thanks to its simple working process while allowing the obtainment of high precision functional parts [2, 3]. 3D bioprinting is of special interest in the biomedical and pharmaceutical fields, due to the offered high degree of personalization. This technology has shown great potential in many applications in these fields, such as for drug delivery, wound dressing, tissue engineering, and customized implants, among others [4–8].

However, for inks to be valid for liquid extrusion 3D printing, they must meet certain criteria [2, 9], and developing new materials valid for DIW and of interest for the aforementioned fields is necessary. Among different studied polymers, waterborne polyurethane–ureas (WBPUUs) have shown potential for this type of 3D printing [10, 11]. Polyurethane–ureas (WBPUUs) are very interesting polymers whose properties can be easily customized; thus, they are used in many diverse applications [12]. Waterborne polyurethane–ureas (WBPUUs) have shown biocompatibility and potential to be used in the biomedical field [13–15]. Moreover, and willing to contribute to the environmental state of the planet, biobased WBPUUs can be prepared by substituting conventional precursors with reactants obtained

✉ Izaskun Larraza
izaskun.larraza@ehu.eus

✉ Aitor Arbelaiz
aitor.arbelaiz@ehu.eus

1 'Materials + Technologies' Research Group (GMT), Department of Chemical and Environmental Engineering, Faculty of Engineering of Gipuzkoa, University of the Basque Country, Pza Europa 1, 20018 Donostia-San Sebastian, Spain

2 Centro de Investigação de Montanha (CIMO), Instituto Politécnico de Bragança, Campus de Santa Apolónia, 5300- 253 Bragança, Portugal

3 Laboratório Associado para a Sustentabilidade e Tecnologia em Regiões de Montanha (SusTEC), Instituto Politécnico de Bragança, Campus de Santa Apolónia, 5300-253 Bragança, Portugal

Published online: 20 September 2023

from natural sources [16]. Moreover, the properties of the WBPUUs and its inks can be modified and enhanced by the addition of additives, as is the case of cellulose nanoentities [17, 18], such as CNF or cellulose nanocrystals (CNC) [19, 20].

However, when inserting printed parts into the human body, there is a big risk of infection. A possible way to reduce this risk could lay in designing new functionalized materials that could confer antibacterial behavior to the printed parts, which could be achieved using natural extracts. Natural extracts are substances that have been used for thousands of years in traditional folk medicine as treatment for infectious diseases [21, 22]. They can be obtained from diverse plants (including different parts of said plants), granting plant extract with a wide range of structures and properties. Plants are rich sources of bioactive compounds, mainly alkaloids, flavonoids, tannins and other phenolic compounds [23, 24]. The bioactive properties shown by these extracts can usually be attributed to phytoalexins, secondary metabolites synthesized by plants to avoid insect, fungal, and microbial infections [25–27]. Natural extracts often show multidirectional biological properties such as antioxidant, anti-inflammatory, anti-allergenic, antitumor, anticancer and antimicrobial activities [27, 28], while still presenting biocompatible behavior [27, 29, 30].

In the fight against bacterial infections, traditional treatments with antibiotics have started to lose effectiveness due to the growing resistance of many strains to these treatments [27]. As a response to this problem, the use of plant extracts in common medicine as an approach to fight bacterial infections is being studied. Plant extracts have shown a low risk of rising resistance from microorganisms. Moreover, plant extracts have also shown a synergetic effect with traditional pharmacological agents, further enhancing their effectiveness [27]. In recent years, there has been increasing use of extracts in biomaterials. Among natural extracts, H*aematoxylum campechianum* L., *Castanea sativa* L. and *Rhamnus frangula* L., also known as logwood, chestnut and alder buckthorn, present antioxidant, antimicrobial, antiviral, antifungal, antitumor and anticancer properties [31–35]. Using these additives in polymeric materials could result in composites with great potential, benefiting from the good thermal and mechanical properties supplied by the polymer matrix and the bioactive behavior given by the added extracts. The use of natural extracts in biomedical applications, such as in tissue engineering, has been described, and their effect on the proliferation and cellular adhesion has been studied [36–39]. Furthermore, the water solubility of aqueous-extracted natural extracts makes them a perfect pairing with water-based polymers, as is the case of WBPUUs.

In this work, bioactive inks for DIW 3D printing are prepared by adding natural extracts to a waterborne polyurethane–urea matrix. For this, three types of natural extracts are used, namely, logwood, chestnut and alder buckthorn extracts, which were added in different contents and following different incorporation routes. The prepared inks were characterized regarding their stability and their rheological behavior. Furthermore, inks were used to produce 3D printed parts, and the properties and antibacterial behavior of the printed parts were characterized.

2. Experimental

2.1. Materials

Renewable sourced difunctional polyol used in the polyurethane–urea synthesis (Priplast 3192®, Mw = 2000 g mol^{-1}) was purchased from Croda. Isophorone diisocyante (IPDI, DESMODOUR I) was kindly supplied from Covestro and ethylene diamine (EDA) was provided by Fluka. 2,2-Bis(hydroxymethyl)propionic acid (DMPA, Aldrich) and triethylamine (TEA, Fluka) were used as internal emulsifier and neutralizing agent, respectively. Dibutyltin dilaurate (Aldrich) was used as catalyst.

Natural plant-based extracts, also used as colorants, namely C11 - logwood extract, C15 - chestnut extract, and C25 - alder buckthorn were purchased from Couleurs de Plantes. Freeze-dried CNF (Lot. 9004-34-6) were provided by the University of Maine.

2.2. Synthesis of the Waterborne Polyurethane–Urea (WBPUU)

A waterborne polyurethane–urea, with a molar ratio of polyol/DMPA/IPDI/EDA of 1/1.1/3.5/0.6, was synthesized using a two-step polymerization procedure. The synthesis was carried out in a 500 mL four-necked jacketed reactor equipped with a mechanical stirrer, thermometer and nitrogen inlet. In the first step the prepolymer, formed by the polyol, the diisocyanate and the catalyst, was synthesized. The mixture was left to react for 1 h at 80 °C under constant mechanical stirring. The reaction was then cooled down to 50 °C and the DMPA and the neutralizing TEA were added dissolved in acetone and left to react for 15 min. For the second step, the reaction was cooled down to room temperature, and the phase inversion step was carried out by dropwise addition (5 mL s^{-1}) of deionized water under vigorous stirring. Finally, the chain extender was added (0.3 mL s^{-1}) to the reaction at 35 °C and left to react for 2 h. An aqueous dispersion of WBPUU was obtained. The progress of the reaction was monitored by the dibutylamine back titration method according to the ASTM D 2572-97.

2.3. Preparation of WBPUU/Natural Extracts Inks

For inks preparation, first the viscosity of the systems was modulated by varying the solid content of the WBPUU dispersion. At a solid content of 50 wt% the WBPUU dispersion ($WBPUU_{50}$) started showing gel-like behavior and this solid content was selected to prepare inks for DIW. Inks were prepared by two methods, ex-situ or in-situ addition of the natural extracts.

In ex-situ preparations, 1, 3 and 5 wt% of extract was added to the already synthesized WBPUU by mechanical stirring, until homogeneous dispersions were obtained. Ex-situ prepared inks were named "xLW_{EX}", "xCN_{EX}" and "xAB_{EX}" for composite inks containing logwood, chestnut or alder buckthorn extracts, respectively, where the "x" refers to the extract content relative to the dried WPUU weight, as specified on Table 1.

For in-situ preparations, the natural extracts were first dispersed in water, and added during the phase inversion step of the synthesis. Since the addition of the natural extract during the synthesis process had a strong effect on the dispersion's homogeneity and viscosity, in some cases the total solid content needed to be readjusted.

For logwood and alder buckthorn extracts, first dispersions with 3 wt% of natural extract were prepared with a total solid content of 50 wt%, and were named $3LW_{IN}$ and $3AB_{IN}$, respectively. However, when higher contents of extract were added (5 wt%) at 50 wt% WBPUU, the viscosity strongly increased, impeding a correct stirring and, thus, dispersions with poor homogeneity were obtained. Hence, in order to solve this constraint, it was necessary to slightly decrease the polyurethane–urea solid content to lower values. After a refinement, this content was set to 47.5 wt%. Inks prepared with 5 wt% of logwood and alder buckthorn extracts at a total solid content of 47.5 wt% were named $5LW_{IN}$ and $5AB_{IN}$, respectively. The compositions of the in-situ prepared inks are shown on Table 2.

Table 2 WBPUU and natural extract contents for in-situ inks preparation

Sample	WBPUU content (wt%)	LW content (wt%)	AB content (wt%)	CNF content (wt%)
$3LW_{IN}$	50.0	3	–	–
$5LW_{IN}$	47.5	5	–	–
$5LW_{IN}2CNF$	47.5	5	–	2
$3AB_{IN}$	50.0	–	3	–
$5AB_{IN}$	47.5	–	5	–
$5AB_{IN}2CNF$	47.5	–	5	2

In order to further modulate the rheology of the inks and improve their behavior for DIW 3D printing, CNF were added to the inks containing the lowest total solid contents (47.5 wt%). For this, 2% of CNF, regarding the total ink weight, was added by mixing under vigorous mechanical stirring using an ultraturrax homogenizer (Polytron PT 2500E, KINEMATICA), at 12,000 rpm for 10 min. $5LW_{IN}$ and $5AB_{IN}$ inks with CNF were name $5LW_{IN}2CNF$ and $5AB_{IN}2CNF$, respectively.

It is worth noting that the addition of chestnut extract during the synthesis process strongly destabilized the formation of a homogeneous dispersion, resulting in an extremely high viscosity phase with observed phase separation. Complex polyphenolic molecules of chestnut extract, mainly tannins with a very high amount of hydroxyl and carboxylic groups, can destabilized the system, as suggested by literature, where excessive contents of carboxylic groups resulted in poorer dispersion stability [40]. The preparation of in-situ added chestnut extract containing inks was discarded due to the poor dispersion capacity observed for these systems.

Table 1 WBPUU and natural extract contents for ex-situ inks preparation

Sample	WBPUU dispersion (g) (50.4 wt%)	WBPUU (g)	Logwood extract (g)	Chestnut extract (g)	Alder Buckthorn extract (g)
$WBPUU_{50}$	20.0	10.08	–	–	–
$1LW_{EX}$	20.0	10.08	0.10	–	–
$3LW_{EX}$	20.0	10.08	0.31	–	–
$5LW_{EX}$	20.0	10.08	0.53	–	–
$1CN_{EX}$	20.0	10.08	–	0.10	–
$3CN_{EX}$	20.0	10.08	–	0.31	–
$5CN_{EX}$	20.0	10.08	–	0.53	–
$1AB_{EX}$	20.0	10.08	–	–	0.10
$3AB_{EX}$	20.0	10.08	–	–	0.31
$5AB_{EX}$	20.0	10.08	–	–	0.53

2.4. Preparation of 3D Printed Parts

- 3D printed parts were obtained from the selected inks, using an adapted DIW Voladora Tumaker printer (a model of which is shown in Fig. 1), in which the inks were placed in a syringe with a 0.8 mm nozzle and were extruded by a mechanically operated piston. 3D printing was carried out at room temperature, at a printing speed of 6 mm s^{-1}.
- As a design, a cylinder with a dimeter of 10 mm and a height of 5 mm was chosen. Obtained parts were freeze-dried right after printed and were labeled as "3D-X", where "X" refers to their corresponding ink.

3. Characterization Techniques

Particle size and stability of the WBPUU dispersions were measured by dynamic light scattering and zeta potential tests, respectively, using a Zetasizer Ultra from Malvern panalytical. The intensity of dispersed light was measured using a luminous source of HeNe laser (wavelength 632.8 nm, 10 mW) and measuring at an angle of 174.7°. Samples were prepared mixing a small amount of aqueous dispersion with ultrapure water and measurements were carried out at 25 °C.

Rheological characterization of WBPUU dispersion and natural extracts containing inks was performed using a Haake Viscotester iQ (Thermo Scientific). Tests were performed at 25 °C and the employed geometry was chosen depending on the viscosity of the ink. Either a coaxial cylinder geometry (CC25 DIN/Ti adapter), with a piston radius of 12.54 mm and a ring gap of 1.06 mm, or a plate-plate geometry (P35/Al adapter), with a diameter of 35 mm and a gap of 1 mm were used.

For flow tests, shear rate sweeps from 0.2 to 1000 s^{-1} were performed. Flow index, n, of each ink was calculated from Power Law (Eq. 1).

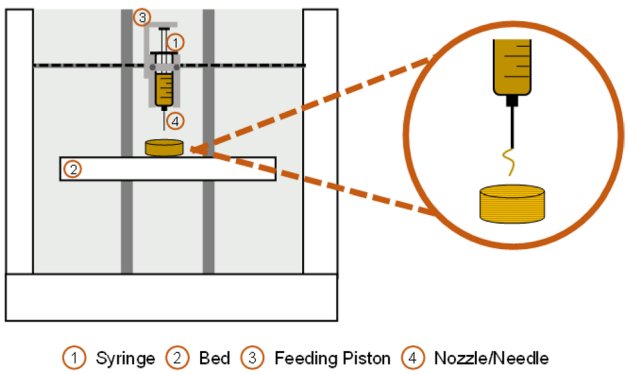

Fig. 1 Schematic model of employed DIW 3D printer

$$\eta = K\dot{\gamma}^{n-1} \quad (1)$$

where η is the viscosity (Pa·s), $\dot{\gamma}$ is the shear rate (s^{-1}), K is the consistency index (Pa·s^n) and n is the flow index (dimensionless).

For yield point determination tests, dynamic oscillatory tests were performed in a shear stress range of 10 up to 10,000 Pa. Yield point was determined as the point of deviation of G′ from linearity, as proposed by Cyriac et al. [41]. Flow point, on the other hand, was measured as the crossover point for G′ and G″. In order to consider statistical relevance of the measured rheological parameters, one way ANOVA was carried out with Excel, at a significant level of $p < 0.05$.

The morphology of the 3D printed and freeze-dried scaffolds was observed by scanning electron microscopy (SEM), using Field Emission Gun Scanning Electron Microscopy (FEG-SEM) Hitachi S-4800 N, at a voltage of 5 kV. Prior to the test, and in order to analyze the cross section of the prepared scaffolds, the samples were cryofractured in liquid nitrogen and sputter coated with a thin layer of gold (~ 10 nm) in an Emitech K550X ion sputter.

The characteristic functional groups of the used natural extracts and the 3D printed WBPUU and composites parts were analyzed by Fourier transform infrared spectroscopy (FTIR) using a Nicolet Nexus spectrometer (Thermofisher Scientific) provided with a MKII Golden Gate accessory (Specac) with a diamond crystal at a nominal incidence angle of 45° and ZnSe lens. Spectra were recorded in attenuated total reflection (ATR) mode between 4000 and 650 cm^{-1} averaging 32 scans with a resolution of 4 cm^{-1}.

The mechanical properties of the 3D printed samples were studied by compression tests, using an Instron 5967 universal testing machine provided with a 500 N load cell. Compression force was applied in the normal direction to the printed layers. Cylindrical samples (Ø=10 mm and h = 5 mm) were compressed at a crosshead speed of 10 mm min^{-1} to a fixed deformation of 60%.

Compression modulus was calculated as the slope of the stress-strain curve at low deformations, the stress was measured at the maximum applied strain (60%) and densification strain as the strain at the intersection point between the stress plateau and a line extrapolated from the densification domain. Moreover, specific Young modulus values were measured as the ratio between each sample's Young modulus and its density, calculated as the ratio between their measured weight and volume. Compression values were averaged for five specimens.

The antibacterial behavior of the WBPUU and the natural extracts containing composites was studied using the Kirby–Bauer modified test. For this, antibacterial assays were performed using Gram-positive bacteria, Staphylococcus aureus ATCC 19,213, and Gram-negative bacteria,

Escherichia coli ATCC 10,536. Briefly, the bacteria inoculums were prepared by aseptically transferring 4 isolated colonies of each microorganism to separate test tubes containing nutrient broth, then incubated for 24 h at 37 °C. The inoculums were diluted to 0.5 McFarland turbidity standard (corresponding to a concentration of $1.5–3.0 \times 10^8$ CFU/mL) using a sterilized Ringer solution. The concentrations of the bacteria dilutions were also controlled by UV–visible spectrophotometry by measuring the absorbance at 625 nm. Then, the bacteria solutions were inoculated in Mueller Hinton Agar plates using a sterilized swab. Afterward, each sample was placed in the center of the plate, and the plates were incubated at 37 °C for 24 and 96 h. After the incubation time, systems were studied and their antibacterial behavior was assessed as follows: in the case of a present inhibition halo (i.e. the bacteria being killed), systems were considered bactericidal; in the case of no halo, but no growth over the surface of the samples, systems were considered as bacteriostatic; last, where there was bacterial growth on the systems, no antibacterial capacity was determined. For sample preparation, WBPUU/natural extracts composite samples with a diameter of 6 mm were used after freeze-dried. To study the behavior of just the active ingredient, natural extracts were used directly. For this, solutions containing the same extract mass as their composite counterparts were prepared and placed on a paper filter disc with a diameter of 6 mm, which were left to dry. As the positive control, antibiotic discs with a 6 mm diameter were used.

4. Results and Discussion

4.1. Characterization of WBPUU/Natural Extracts Inks

In order to assess the potential of the prepared inks, first the stability of the synthesized dispersions was studied, since the high solid content of the WBPUU dispersions could have a negative impact on the stability of the systems [42, 43]. In order to analyze this effect, the particle size and zeta potential of the prepared 50 wt% WBPUU and in-situ prepared inks were analyzed. The obtained values are shown in Table 3.

All systems showed a similar particle size, with a diameter of around 130 nm. These values are similar to those determined for the same formulation at lower solid contents [18] and those reported in literature [44–46]. The high solid content and addition of natural extract did not significantly affect this property of the WBPUU dispersions. When analyzing the effect of the solid content and extract incorporation on the stability of the systems, it can be observed that all systems still present good stability, with zeta potential values far from the required limits for stable dispersions, above + 30 mV or below − 30 mV [47].

Table 3 Particle size and Z-potential values for high solid content WBPUU dispersions

Sample	Particle size (nm)	Z-potential (mV)
$WBPUU_{50}$	130.1 ± 4.4	− 51.0
$3LW_{IN}$	118.5 ± 6.5	− 51.9
$5LW_{IN}$	126.7 ± 4.0	− 53.0
$3AB_{IN}$	140.2 ± 9.7	− 47.9
$5AB_{IN}$	133.1 ± 5.7	− 49.0

The obtained results proved that neither the high solid contents nor the addition of natural extract resulted in unstable dispersions. Systems showed small enough particle size that allowed the formation of a thick electrochemical double layer and, thus, were able to remain suspended, and show stable zeta potential values.

The potential of the prepared inks for DIW 3D printing was studied through rheological characterization tests. There are two relevant parameters when studying the potential of an ink for DIW, their printability and their shape fidelity. The printability of an ink refers to its capacity to be continuously extruded, whereas the shape fidelity refers to its capacity to retain the given shape while supporting the weight of the top layers. Ideal inks for 3D printing must show shear-thinning behavior, in order to flow under applied stress (during printing), but maintain their shape at rest (after deposited). Moreover, and for the same reason, they must show defined but not too high yield points. The values of viscosity and storage modulus will also play a big role on the printing capacity of the materials.

For rheological tests, $5LW_{IN}$ ink measurements were carried out with a concentric cylinder geometry, due to its low viscosity, whereas other inks were studied using a plate-plate geometry. Viscosity vs. shear rate curves for ex-situ and in-situ prepared inks are shown in Fig. 2. Moreover, Table 4 summarizes the viscosity values of the inks at different shear rates and the n value calculated from Power Law (Eq. 1).

For the viscosity measurement of the inks at the printing rate, first, the shear rate of the inks in the nozzle, $\dot{\gamma}_n$, was calculated. For this, the non-Newtonian behavior of the inks and, thus, their non-parabolic velocity profile was taken into account. Therefore, the shear rate on the nozzle was calculated using the equation proposed by Li et al. [13] (Eq. 2).

$$\dot{\gamma}_n^n = \left[\frac{V \bullet R^2}{\left(\frac{n}{3n+1}\right)\left(R^{\frac{3n+1}{n}}\right)} \right]^n \bullet r \tag{2}$$

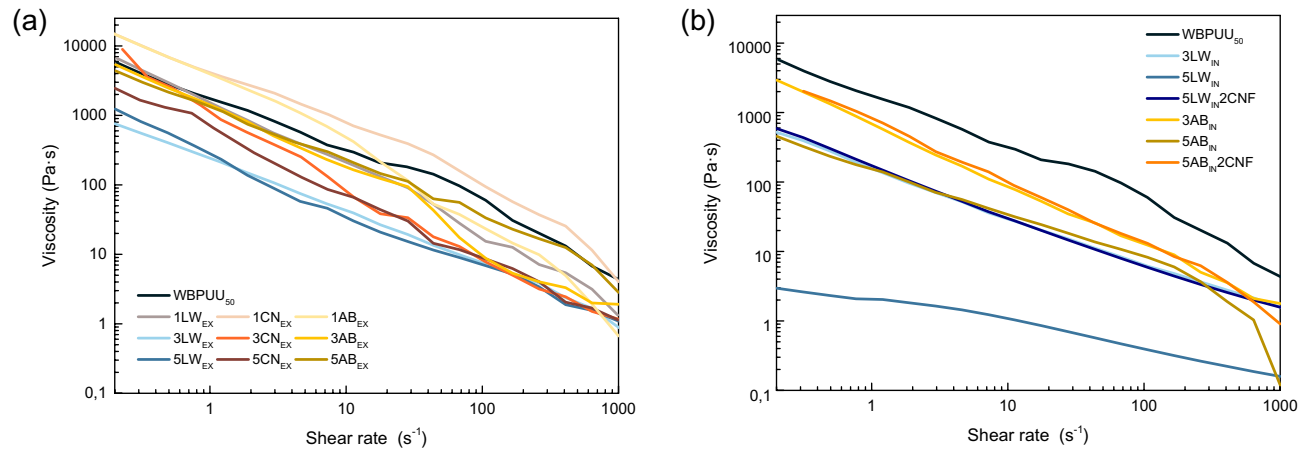

Fig. 2 Viscosity as a function of shear rate of **a** ex-situ and **b** in-situ prepared WBPUU and natural extracts containing inks

Table 4 Rheological parameters measured for ex-situ and in-situ prepared WBPUU and natural extracts containing inks

	Sample	η at 0.02 s^{-1} (Pa·s)	η at γ_n (Pa·s)	η at 100 s^{-1} (Pa·s)	n	Yield point (Pa)	Flow point (Pa)
	$WBPUU_{50}$	7598.1 ± 926.0	481.1 ± 49.2	56.0 ± 11.3	0.189	609.0 ± 63.3	2567.6 ± 86.5
ex-situ	$1LW_{EX}$	6578.5 ± 134.3	1753.9 ± 197.4*	16.1 ± 0.8*	0.056	253.4 ± 40.2*	1663.3 ± 44.1*
	$3LW_{EX}$	1094.3 ± 472.7*	57.9 ± 4.8*	6.4 ± 1.7*	0.166	40.7 ± 20.0*	254.6 ± 122.6*
	$5LW_{EX}$	1021.4 ± 299.1*	48.2 ± 3.6*	6.4 ± 1.1*	0.168	23.4 ± 4.4*	120.7 ± 15.7*
	$1CN_{EX}$	14984.8 ± 201.6*	1647.3 ± 479.3	85.9 ± 21.1	0.197	985.6 ± 41.3*	5524.2 ± 47.2*
	$3CN_{EX}$	5577.3 ± 1577.5	219.2 ± 58.5*	8.8 ± 0.7*	0.068	97.0 ± 16.5*	892.0 ± 359.6*
	$5CN_{EX}$	2454.9 ± 184.1*	220.0 ± 22.4*	9.0 ± 0.2*	0.08	16.3 ± 3.0*	111.8 ± 112.2*
	$1AB_{EX}$	14524.1 ± 732.1*	1394.7 ± 221.3*	24.8 ± 2.5	0.066	476.9 ± 19.6	3988.3 ± 232.1*
	$3AB_{EX}$	5704.2 ± 457.2	533.9 ± 51.4	9.6 ± 1.4*	0.053	373.8 ± 124.5	2310.9 ± 498.4
	$5AB_{EX}$	4867.3 ± 719.6	996.2 ± 30.0*	36.1 ± 4.2	0.228	188.9 ± 27.2*	1986.0 ± 28.7*
in-situ	$3LW_{IN}$	536.8 ± 25.0*	29.9 ± 3.0*	5.4 ± 0.9*	0.289	89.8 ± 48.0*	283.4 ± 147.3*
	$5LW_{IN}$	2.3 ± 0.8*	0.6 ± 0.1*	0.4 ± 0.0*	0.658	–	–
	$5LW_{IN}$ 2CNF	1061.9 ± 492.7*	17.9 ± 4.9*	3.3 ± 1.1*	0.308	38.6 ± 6.4*	109.5 ± 50.0*
	$3AB_{IN}$	2814.1 ± 163.5*	145.7 ± 16.3*	12.3 ± 0.9*	0.123	266.6 ± 45.5*	837.5 ± 108.6*
	$5AB_{IN}$	626.9 ± 244.9*	50.0 ± 10.6*	8.5 ± 0.1*	0.220	61.0 ± 10.1*	220.1 ± 18.9*
	$5AB_{IN}$ 2CNF	2891.0 ± 53.8*	183.0 ± 5.5*	14.2 ± 1.3*	0.132	88.9 ± 7.8*	641.4 ± 82.0*

* symbolizes statistical differences ($p < 0.05$) in respect to the neat polyurethane, i.e. $WBPUU_{50}$

where n is the flow index calculated from Power Law, V is the printing speed, r is any distance between the center of the nozzle and its radius (in this case r = R, to calculate the shear rate on the wall of the nozzle), and R the radius of the nozzle.

All systems showed shear-thinning behavior, with viscosity values dropping at higher shear rates and with n values lower than 1. However, the type and content of added natural extract, as well as the incorporation route, significantly affected the viscosity values of the inks. Overall, it was observed that the higher the extract content was, the lower the ink viscosity was. It must be highlighted that, except for inks with 1% content of either chestnut and alder buckthorn extracts, all the other systems showed lower viscosity values compared to the neat WBPUU ink.

The change of the viscosity could be due to the surfactant effect of the natural extract, as previously reported on literature [48, 49]. The interaction of the surfactant molecules with the polymer macromolecules can increase or decrease the solution's viscosity due to extension, shrinking and bridging of polymer macromolecules. Several factors can affect the surfactant - polymer interactions, being the structure of the surfactant molecules one of them [50].

Regarding the type of extract, logwood containing systems presented lower viscosity values than those exhibited by chestnut or alder buckthorn containing inks. The smaller

molecular size and the lack of carboxylic groups of logwood extract components were beneficial to reach an easier flow. On the other hand, for chestnut and alder buckthorn extracts, due to their bigger and more complex molecules, a different effect was observed. At low extract content, 1 wt%, the incorporated extract amount was not enough to reduce the viscosity of the WBPUU ink, being observed, on the contrary, a slightly viscosity increase. The high concentration of functional groups of the natural extracts components were likely to interact with urethane-urea groups, as well as with the water present in the systems. At this additive content, the surfactant effect of the extracts was not enough to counteract the effect of the formed extract-water interactions and, thus, higher viscosity values were obtained. The high viscosity exhibited by some of the inks may difficult the extrusion process of 3D printed parts.

Regarding the incorporation route, in-situ preparation promoted interactions between the WBPUU and the additives, whereas for ex-situ route, interactions with the water were more likely and, thus, systems with higher viscosities were obtained in this case. For in-situ prepared inks, the hydrophilic groups of the phenolic compounds of the extracts could facilitate the dispersion formation during the synthesis process, and thus dispersions with lower viscosity were obtained.

It is worth mentioning, that, overall, for ex-situ preparations, more statistically sound differences were observed for systems prepared with logwood extracts, whereas alder buckthorn containing systems showed the least significant results. This fact could be due to two factors: (a) alder buckthorn extract producing a lower effect on the properties of the matrix and (b) the poor homogeneity shown by these systems, resulting in bigger deviations of the measured values. On the other hand, all in-situ prepared inks presented statically relevant changes compared to the matrix, as well as lower standard deviation values, proving that a higher homogeneity was achieved by this preparation route.

$5LW_{IN}$ and $5AB_{IN}$, due to their lower solid content, showed significantly lower viscosities, which increased with CNF addition. Cellulose, as reported in literature [51, 52], can be used to modulate inks' viscosities and, thus, improve 3D printing process.

Spectromechanical analyses were performed in order to analyze the gel behavior of each ink under applied stress. Figure 3 shows storage and loss moduli vs. shear stress curves for ex-situ and in-situ prepared inks. Moreover, yield and flow points were measured and are shown on Table 4.

As can be observed, the addition of natural extracts reduced, in general, the gel-like strength of the systems, resulting in an overall decrease of the yield and flow point, as well as in a decrease of the storage and loss moduli values in the linear zone. The results determined by flow tests, pointed out that logwood containing inks have a weaker gel-like behavior, being these inks the ones more willing to flow. In the case of in-situ prepared inks, they presented even lower yield and flow points, possibly derived from the strong surfactant effect of the natural extracts favored by this incorporation method facilitating the dispersion formation, thus resulting in systems with weaker gel-like behavior. $5LW_{IN}$ (Figure S1) did not show a gel-like structure, due to its low solid content and the strong surfactant effect caused by the used 5 wt.% logwood extract. However, the addition of cellulose changed this trend, and effectively increased the yield and flow points of the inks, as well as their G′ and G″ values, proving a strong reinforcing effect.

Nonetheless, the defined yield points and high G′ values observed for all systems, except for $5LW_{IN}$, pointed to a good shape fidelity when used in DIW 3D printing [53].

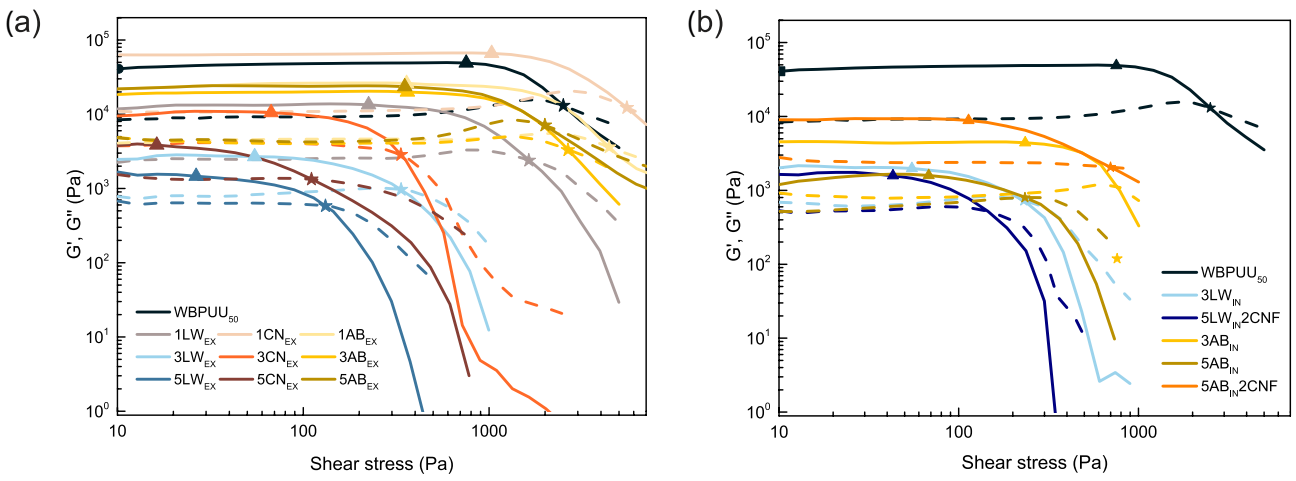

Fig. 3 Storage (solid line) and loss (dotted line) moduli as a function of shear stress and yield (▲) and flow (★) points of **a** ex-situ and **b** in-situ prepared natural extracts containing inks

However, the high yield points shown by some systems, especially in the case of ex-situ prepared inks, might difficult the printability of the inks during the extrusion process.

Overall, most of the prepared systems showed good potential for DIW, showing shear thinning behavior, which would allow their extrusion, and defined yield points, which could result in good shape fidelity of the printed parts.

4.2. 3D Printing and Characterization of Printed Parts

$WBPUU_{50}$ and natural extracts containing inks were used to obtain 3D printed parts by DIW. Initial printability tests were conducted to analyze the effect of the inks' rheology in the 3D printing process. The inks containing 1 wt% of natural extracts, prepared by ex-situ route, showed problems when printing due to their extremely high viscosities and high yield points even at high shear rates. During the extrusion process a discontinuous flow was observed, therefore, it was not possible to successfully obtain 3D printed parts. For higher contents of natural extracts, the inks showed better printability. However, at 5 wt%, some obstruction problems were occasionally encountered. The high amount of natural extracts may have resulted in poorer dispersibility, creating some extract agglomerations, which lead to nozzle obstruction. Overall, inks containing 3 wt% of natural extracts showed the most promising printability. $WBPUU_{50}$ showed significantly better printability than the 1 wt% natural extracts containing inks, the lower viscosity measured under printing shear rate allowed for a more continuous printing process. However, it showed poor shape fidelity, due to the sharp edges and points caused by the high stickiness exhibited by the material.

Considering the initial printability screening tests, inks with a content of 3 wt% of natural extracts were selected to prepare 3D printed objects. 3D printed parts from $5AB_{EX}$ were also obtained, to study the effect of content of natural extracts on the final material. The obtained 3D printed parts are shown in Fig. 4. In general, parts with relatively inaccurate shape fidelity were obtained, as a result of the non-continuous flow and the obstructions formed in the nozzle by agglomerated extracts, as well as due to the high stickiness shown by the inks.

For in-situ preparations, the inks showed better printability, as well as shape fidelity. The better dispersion achieved by this incorporation route impeded the formation of agglomerates, and as consequence, nozzle obstruction was avoided. It is to note that the addition of cellulose significantly improved the printing process, giving rise to the best shape fidelity for both inks containing CNFs.

In order to infer the possible interactions formed between the waterborne polyurethane–urea and the added natural extracts, FTIR analysis was carried out.

Figure 5 shows structures of some of the components found in the extracts used. Among the many components of logwood extract, hematoxylol A, epihematoxylol B and mainly, hematoxylin (Fig. 5a) are the most bioactive compounds [54, 55]. For chestnut extracts, a great variety of components are found, being tannins and some other phenolic compounds the principal components, namely vescalin, castalin, gallic acid, vescalagin, castalagin, kurigalin, acutissimin A and ellagic acid (Fig. 5b) [31, 56]. In alder buckthorn extract, structures such as anthraquinones, among

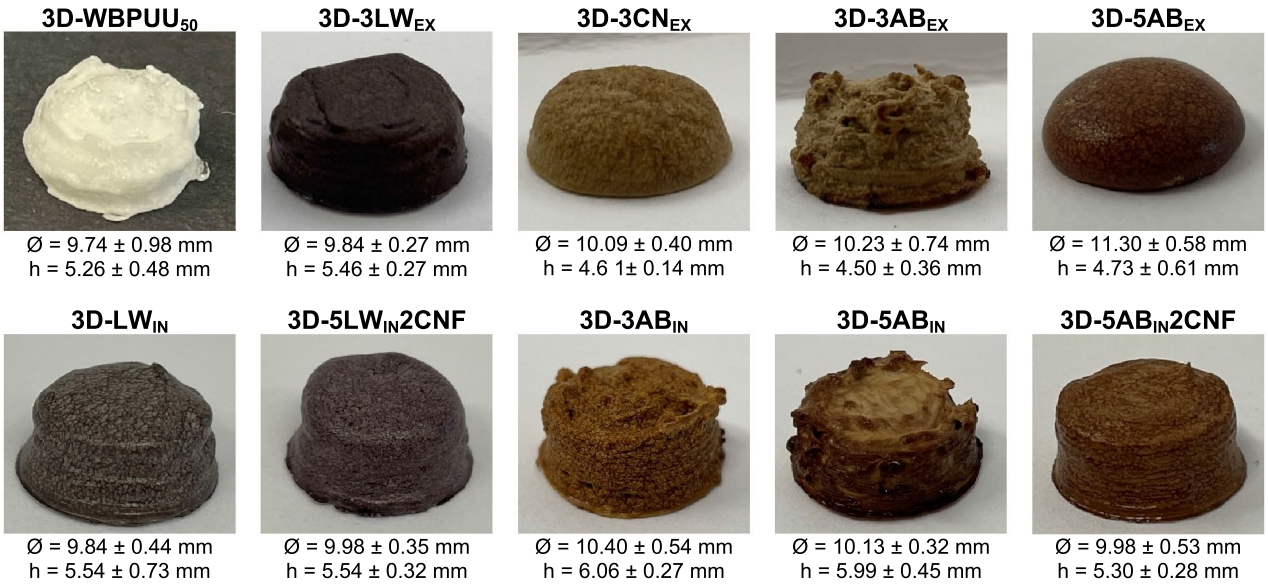

Fig. 4 Photographs of 3D printed cylinders obtained from $WBPUU_{50}$ and natural extracts containing inks

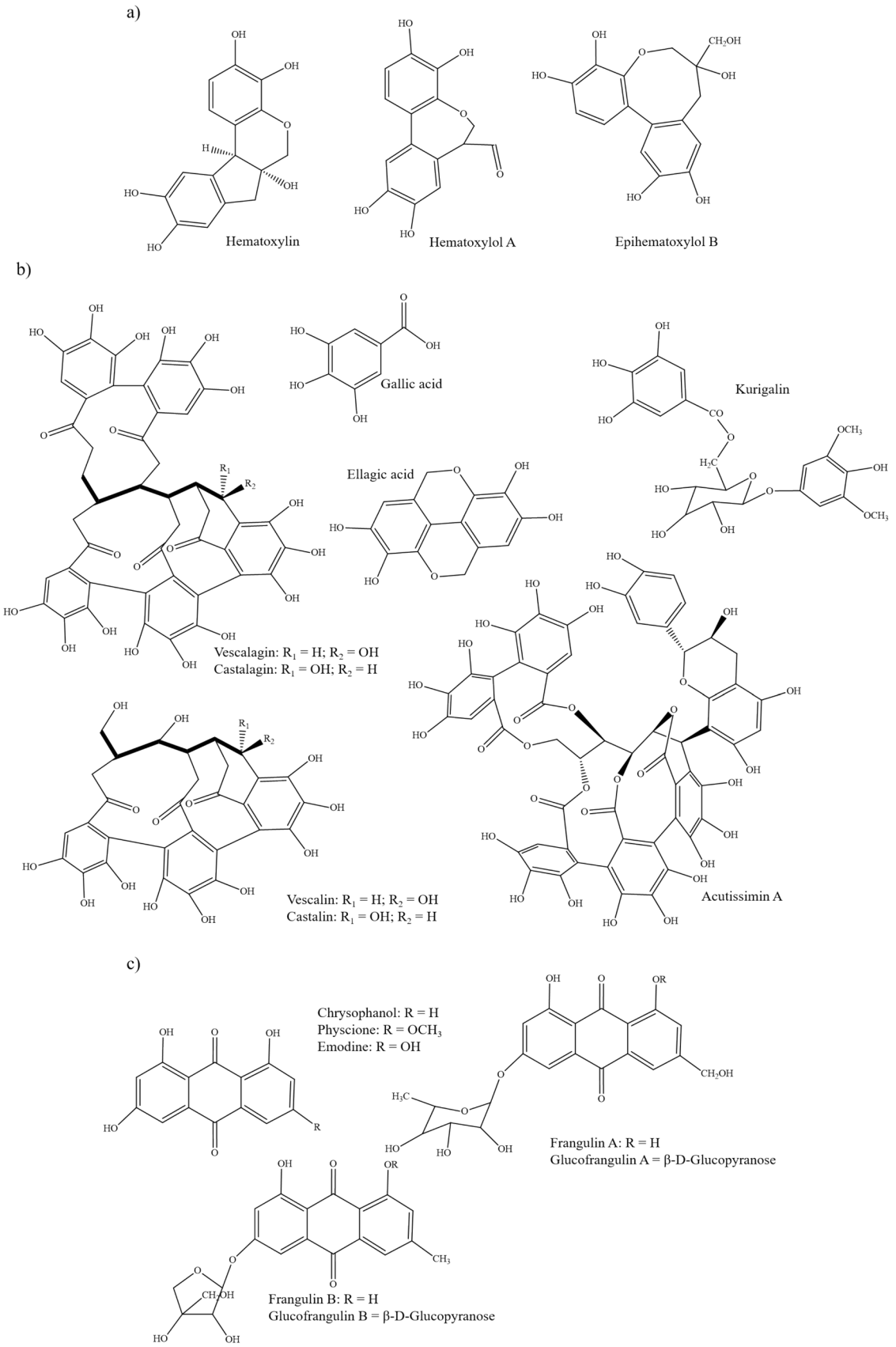

Fig. 5 Structures of some on the components found in **a** logwood, **b** chestnut and **c** alder buckthorn extracts

them, chrysophanol, physcione and emodine [33, 57], and some other important constituents, such as frangulin A and B and glucofrangulin A and B (Fig. 5c), are found [58].

The spectra of the natural extracts and the 3D printed parts are shown in Figs. 6 and 7, respectively.

The spectra of logwood, chestnut, and alder buckthorn extracts showed a wide band between 3700 and 3000 cm^{-1}, related to the O–H groups of the many phenolic groups present on their structure [59]. The bands present in the 1600−1500 cm^{-1} range were attributed to the C=O, and the C=C of the aromatic rings [60, 61]. Moreover, for chestnut and alder buckthorn extracts, a band related to the carbonyl groups was also assigned around 1720 cm^{-1}, which was less evident for logwood extract, indicating a lower carbonyl group content.

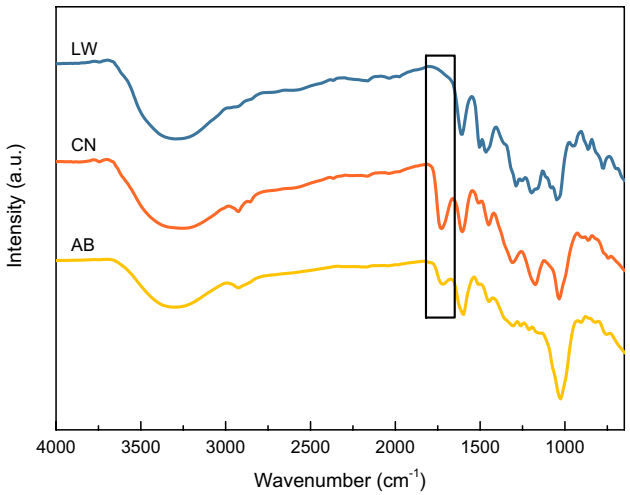

Fig. 6 FTIR spectra of logwood, chestnut and alder buckthorn extracts

3D-$WBPUU_{50}$ showed all the characteristic bands of polyurethane–ureas, being the most representative bands those of the stretching vibration of N–H and C=O of urethane and urea groups, located in the 3500−3100 cm^{-1} and 1800−1600 cm^{-1} ranges, respectively. Other bands were also observed related to the symmetric and asymmetric stretching vibration of the C–H bonds at 2927 and 2858 cm^{-1}, respectively, the C–N stretching vibration and N–H bending of urethane and urea groups at 1545 cm^{-1} in amide II region, and the C–O–C stretching vibration between 1250 and 1000 cm^{-1} [16, 18].

When analyzing the spectra of the ex-situ prepared composites (Fig. 7a), it can be observed that, in general, the addition of the natural extracts did not shift the spectra bands in comparison to the neat 3D-$WBPUU_{50}$. However, an increase in the N–H band intensity was observed with the addition and content of extracts (Fig. 7 inset), attributed to the overlapping of the N–H band of the polyurethane–urea with the O–H band pertaining to the natural extracts. In the FTIR spectra of the composites obtained from in-situ prepared inks (Fig. 7b), besides the N–H band intensity increase, a shift towards lower wavenumbers was also observed, more intense at higher extract contents and when CNFs were added. The band, centered at 3362 cm^{-1} in 3D-$WBPUU_{50}$ spectrum, went down to 3346 and 3350 cm^{-1}, for $5LW_{IN}2CNF$ and $5AB_{IN}2CNF$, respectively. This shift suggested the formation of interactions, both chemical and physical, between the polyurethane–urea matrix and the natural extracts, which are favored in in-situ preparation, as well as when cellulose nanofibers are used [62] .

The morphology of the 3D printed parts was studied by SEM and the micrographs obtained for the ex-situ and in-situ prepared inks are shown in Figs. 8 and 9, respectively. The addition of natural extracts, as well as their origin,

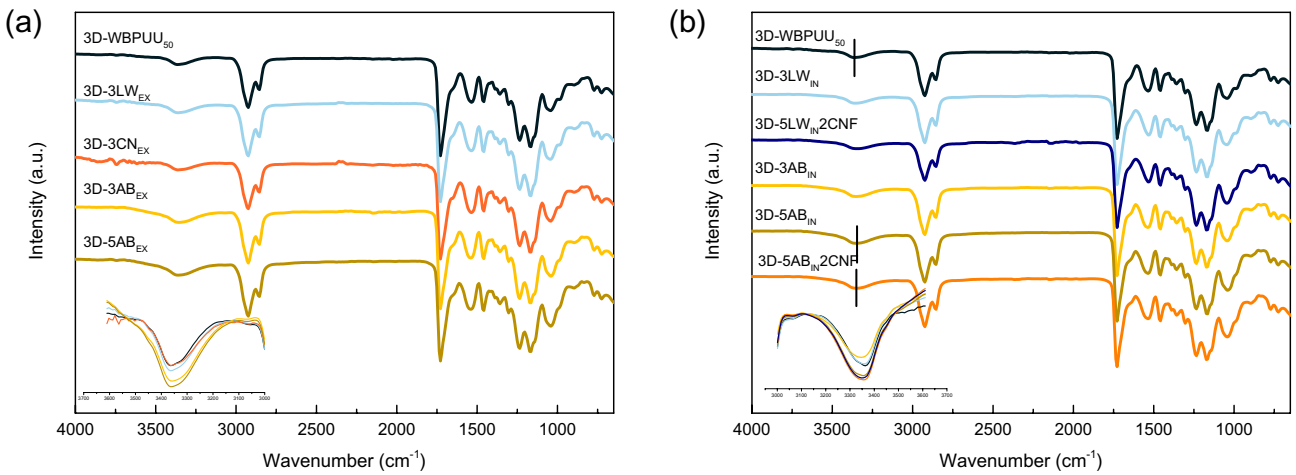

Fig. 7 FTIR spectra of 3D printed parts from $WBPUU_{50}$ and **a** ex-situ and **b** in-situ prepared natural extracts containing inks

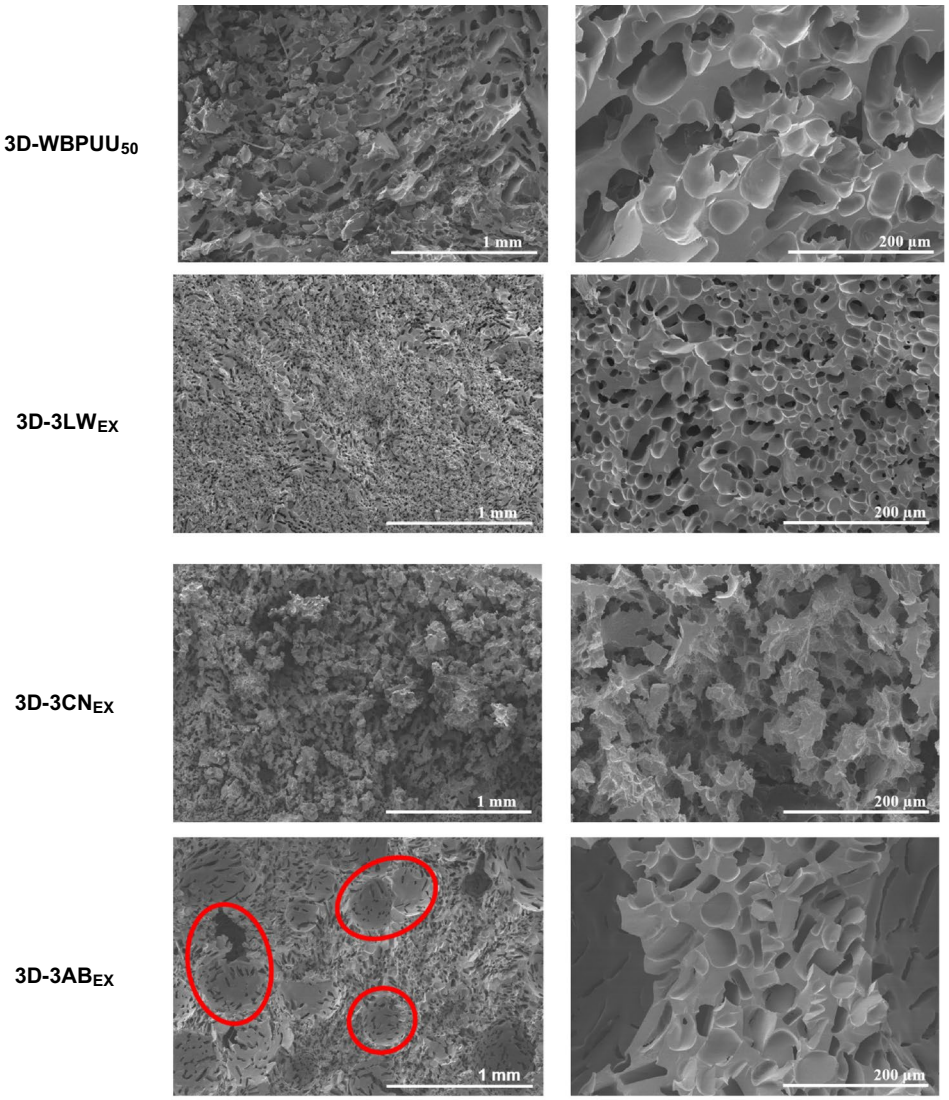

Fig. 8 SEM images of 3D printed parts from WBPUU50 and ex-situ prepared natural extracts containing inks

content, and incorporation route affected the morphology of the final materials.

The part printed from the neat polymer ink, 3D-WBPUU$_{50}$, showed a relatively homogeneous porous structure, formed by spherical pores with an average diameter of 60.2 ± 12.9 µm. In ex-situ prepared composites, the addition of the extracts severely altered this morphology. 3D-3LW$_{EX}$ showed a similar morphology to that of the neat polymer, however, the spherical pores were significantly smaller, with an average diameter of 24.5 ± 3.5 µm. On the other hand, composites containing chestnut and alder buckthorn extracts presented very different morphologies. For 3D-3CN$_{EX}$ a more open wall structure was observed, with fully connected pores. Apparently, 3D-AB$_{EX}$ showed similar pores to those observed in 3D-WBPUU$_{50}$ and 3D-3LW$_{EX}$, however, at lower magnifications, the presence of holes in the structure was clearly evidenced (circled in red in Fig. 8), fact related with the non-continuous printing process shown by the 3AB$_{EX}$ ink, caused by its poor flow and a continuous nozzle obstruction.

In the case of in-situ preparations, the addition of extracts resulted in pore size reduction, which could be attributed to interactions between the polyurethane–urea and the extracts, observed in these systems, resulting in pores diameter of 15.3 ± 2.8 µm for 3D-3LW$_{IN}$ and 34.4 ± 6.5 µm for 3D-3AB$_{IN}$. 3D-3LW$_{IN}$ showed a homogeneous structure with spherical pores, proving the good rheological behavior of this ink, which was able to support the printed structure. However, for 3D-3AB$_{IN}$ the occasional hole in the structured produced by a non-continuous printed process can be found, similar though less frequent than for its ex-situ counterpart (circled in red). For 3D-5AB$_{IN}$, however, a different behavior was observed, resulting in a more heterogeneous morphology. In fact, bottom layers showed elongated pores ($244.2 \pm 30.3 \times 53.0 \pm 6.0$ µm) while upper

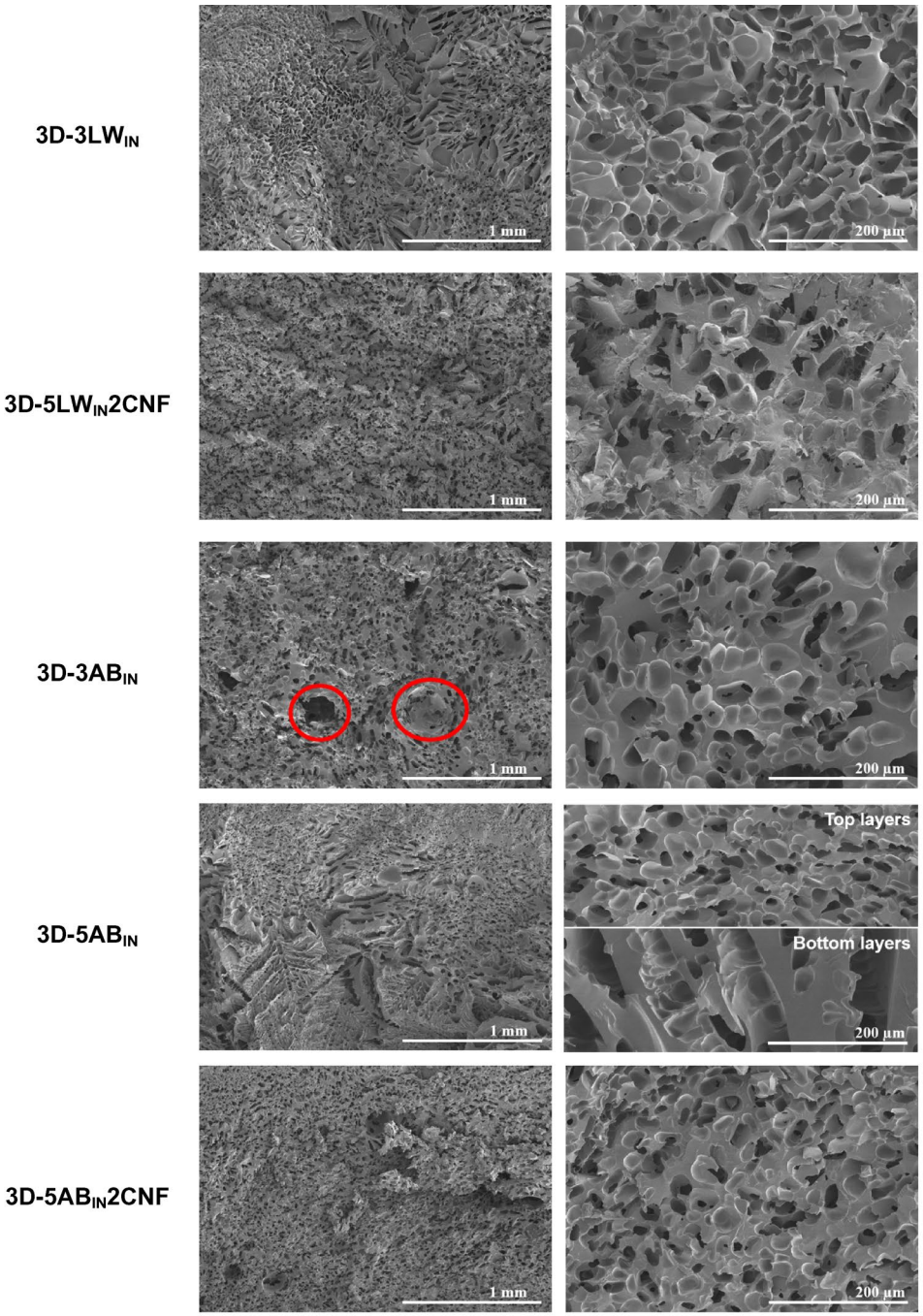

Fig. 9 SEM images of 3D printed parts from in-situ prepared natural extracts containing inks

layers maintained the spherical porous structure (Ø = 16.9 ± 3.9 µm). The lower viscosity and modulus values shown by this system, attributed to its lower solid content, was not enough to support the weight of the layers, causing, the structure of the bottom layers to collapse when additional layers were deposited. The addition of CNF easily solved this problem; for 3D-5AB$_{IN}$2CNF the recovery of the homogeneous spherical porous morphology was observed, with pores showing diameters of 33.6 ± 4.6 µm. For 3D-5LW$_{IN}$2CNF a similar morphology with 38.5 ± 7.9 µm diameter was observed.

The mechanical behavior of the 3D printed parts was analyzed by compression tests. The measured values of Young modulus, density, specific Young modulus, stress at 60% strain and densification strain values are summarized on Table 5, whereas stress/strain curves are shown in Fig. 10.

The addition of the natural extracts strongly affected the mechanical behavior of the polyurethane–urea, increasing

Table 5 Young modulus, specific Young modulus, stress at 60% strain and densification strain values for 3D printed parts obtained from $WBPUU_{50}$ and natural extracts containing inks

	Sample	Young modulus (MPa)	Density (g cm^{-3})	Specific Young modulus (MPa cm^3 g^{-1})	Stress at 60% strain (MPa)	Densification strain (%)
	3D-$WBPUU_{50}$	4.3 ± 0.8	0.35 ± 0.04	12.2 ± 1.8	1.2 ± 0.2	49.3 ± 1.4
ex-situ	3D-$3LW_{EX}$	29.9 ± 3.3	0.44 ± 0.04	66.6 ± 8.8	5.1 ± 0.4	51.1 ± 0.1
	3D-$3CN_{EX}$	13.5 ± 2.2	0.33 ± 0.01	41.1 ± 6.2	2.4 ± 0.5	49.4 ± 0.9
	3D-$3AB_{EX}$	7.1 ± 3.1	0.31 ± 0.03	23.0 ± 8.5	1.4 ± 0.3	49.5 ± 1.2
	3D-$5AB_{EX}$	10.2 ± 2.6	0.37 ± 0.05	27.5 ± 6.0	1.9 ± 0.5	51.4 ± 0.3
in-situ	3D-$3LW_{IN}$	36.9 ± 4.0	0.49 ± 0.03	75.3 ± 5.6	6.3 ± 0.1	49.7 ± 1.2
	3D-$5LW_{IN}$2CNF	64.6 ± 4.7	0.53 ± 0.04	122.0 ± 8.0	9.3 ± 1.0	50.6 ± 0.7
	3D-$3AB_{IN}$	11.6 ± 2.3	0.44 ± 0.05	26.9 ± 8.1	2.6 ± 0.3	50.7 ± 0.8
	3D-$5AB_{IN}$	29.6 ± 4.2	0.46 ± 0.02	65.1 ± 8.9	5.1 ± 0.6	51.9 ± 0.6
	3D-$5AB_{IN}$2CNF	46.8 ± 9.0	0.50 ± 0.03	93.4 ± 12.6	6.8 ± 1.1	51.8 ± 1.3

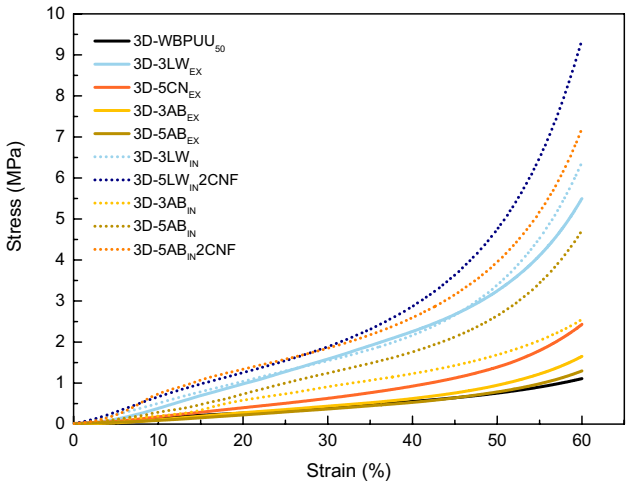

Fig. 10 Stress/Strain curves for 3D printed parts obtained from WBPUU50 and natural extracts containing inks

their Young modulus, specific Young modulus and stress at 60% strain. This data agreed with the reinforcement effect supplied by another plant extract (*Salvia*) reported in a previous work [63]. Results showed that the type, content, and incorporation route influenced the mechanical behavior of the final material. Regarding the extract type, logwood extract gave rise to the stronger reinforcement effect, with composites containing this extract presenting the highest Young modulus and specific Young modulus values, fact related to the better affinity of this extract with the matrix. Chestnut and alder buckthorn extracts also provided rigidity and strength to the systems, but with a less pronounced effect for these formulations.

Analyzing the effect of the incorporation route, in-situ addition route gave rise to materials with higher Young modulus, specific Young modulus and stress values. The higher amount of physical interactions and possible chemical reactions between the polyurethane and the extracts, in addition to the good dispersions achieved, led to improved mechanical properties, which is in agreement with rheological and FTIR data previously reported. The addition of cellulose imparted a further reinforcement, reflected in higher Young modulus and specific Young modulus values, as previously reported on literature for cellulose containing formulations [17].

It is worth noting the significant differences in the density values of the printed parts, especially for ex-situ prepared formulations. This fact is related to the poor printability of the materials, hindering a suitable printing process able to obtain completely filled printed parts, as it was corroborated by the SEM studies.

The antibacterial effect of the natural extracts and its transfer to the polyurethane–urea matrix was evaluated by testing both the natural extracts and the 3D printed parts.

After 1 day of incubation (Fig. 11), pure extracts showed good bactericide behavior against both strains, agreeing with their good reported antibacterial behavior [26–28, 64–67]. Inhibition zones were dependent on the extract type. Logwood extract showed the stronger antimicrobial behavior, with inhibition zones of 22 mm in diameter against *S. aureus*, comparable to the antibiotic (positive control), and 10 mm against *E. coli*. The extract content also affected the bactericide behavior, showing higher antibacterial capacity as it increased. (Supplementary).

3D-$WBPUU_{50}$ showed bacteriostatic behavior against both strains. Even though no inhibition zone was observed, no bacteria growth over the material was observed either. The same effect was also observed for systems containing alder buckthorn extract, 3D-$3AB_{EX}$, 3D-$5AB_{EX}$, 3D-$3AB_{IN}$ and 3D-$5AB_{IN}$. The parts obtained from ex-situ prepared inks containing logwood and chestnut extracts showed bactericide behavior, exhibiting clear inhibition zones. However, for in-situ prepared logwood extract containing

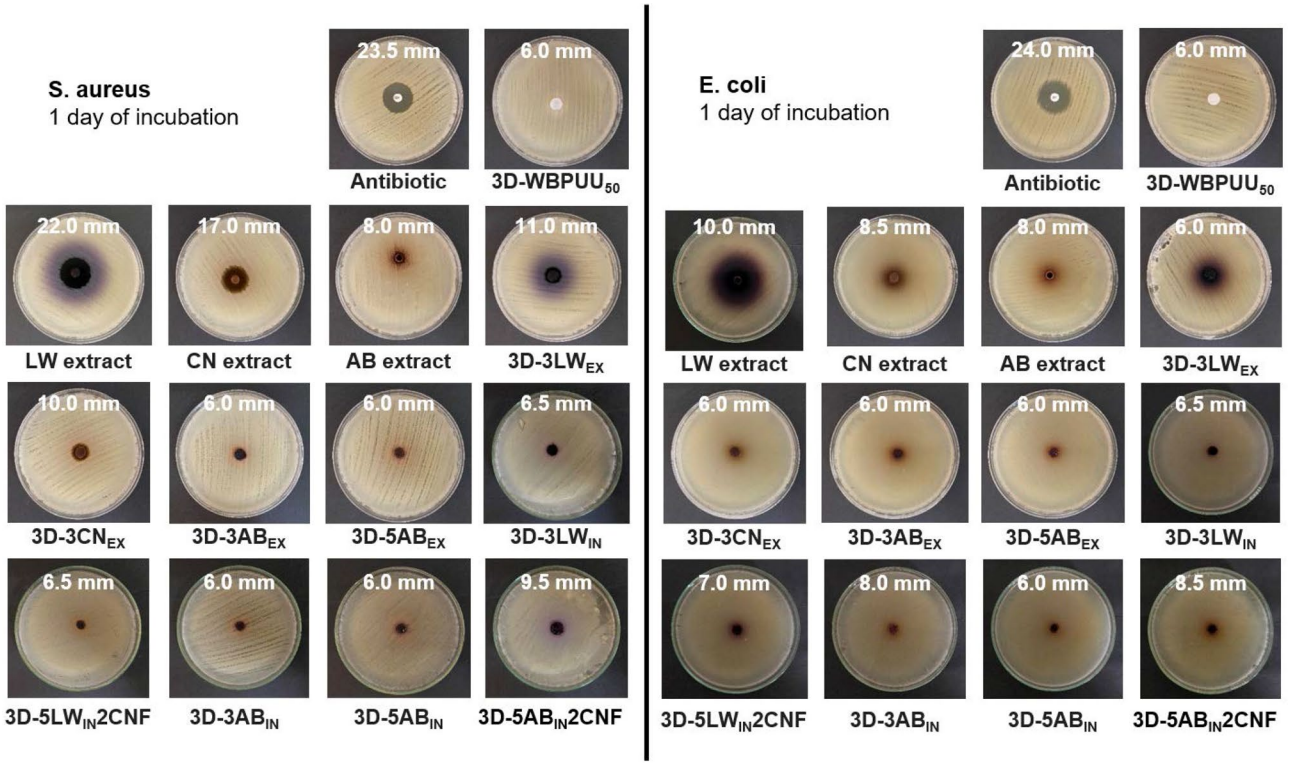

Fig. 11 Antibacterial tests for natural extracts and 3D printed parts against *S. aureus* and *E. coli* after 1 day of incubation at 37 °C

composites, lower inhibition areas were verified, which could be attributed to the entrapment of the extracts inside the polyurethane matrix. Overall, tests against *E. coli* strain showed lower activity, a common fact since gram negative bacteria present a thicker outer lipopolysaccharide membrane [68], which often results in higher antibacterial resistance. All systems exhibited bacteriostatic behavior, with no bacteria growth over the samples. In-situ preparations with CNF showed also bactericide behavior, and the inhibition halos were larger for these systems, agreeing with reports about the antibacterial behavior of cellulose. The effect of the natural extract content was observed, mainly against *S. aureus*, systems with improved bactericide capacity were obtained at higher extract contents (Supplementary).

The capacity to maintain the antimicrobial effect over longer periods was also analyzed. Figure 12 shows the analyzed disks after 4 days of incubation. All the systems showed similar behavior to the corresponding values after 1 day of incubation, proving the antibacterial behavior of the materials over time. For some systems, the inhibition halo even increased after four days, this could be due to a higher release of the natural extracts with time. The good antibacterial behavior exhibited by WBPUU/natural extract composites makes them a promising material for many applications, namely in the biomedical and pharmaceutical fields.

Moreover, Fig. 13 shows a summary of the obtained results. In this figure, the strong effect of the neat extract against *S. aureus* can be clearly observed. This effect is also present against *E. coli*, though less pronounced. The same trend is followed by the printed composites, where the inhibition capacity is stronger against gram-positive bacteria. The weaker behavior of Alder Buckthorn extract is also clearly seen.

5. Conclusions

The capacity to prepare bioactive inks valid for 3D printing using a waterborne polyurethane–urea as matrix and natural extracts as additives was demonstrated, as well as the effect of the type, content and incorporation route of the extracts.

Though all WBPUU-based inks presented shear-thinning behavior, their rheological behavior could be further tuned by the incorporation of additives, which will be crucial in the degree of success of the 3D printing process. In this regard, inks prepared in-situ presented higher homogeneity and allowed a better printability, and CNF containing inks resulted in a better shape fidelity. This fact was also translated in better mechanical behavior, due to a more homogeneous structure and a better stress-transfer. Moreover, amid the bacteriostatic behavior shown by the composites, the

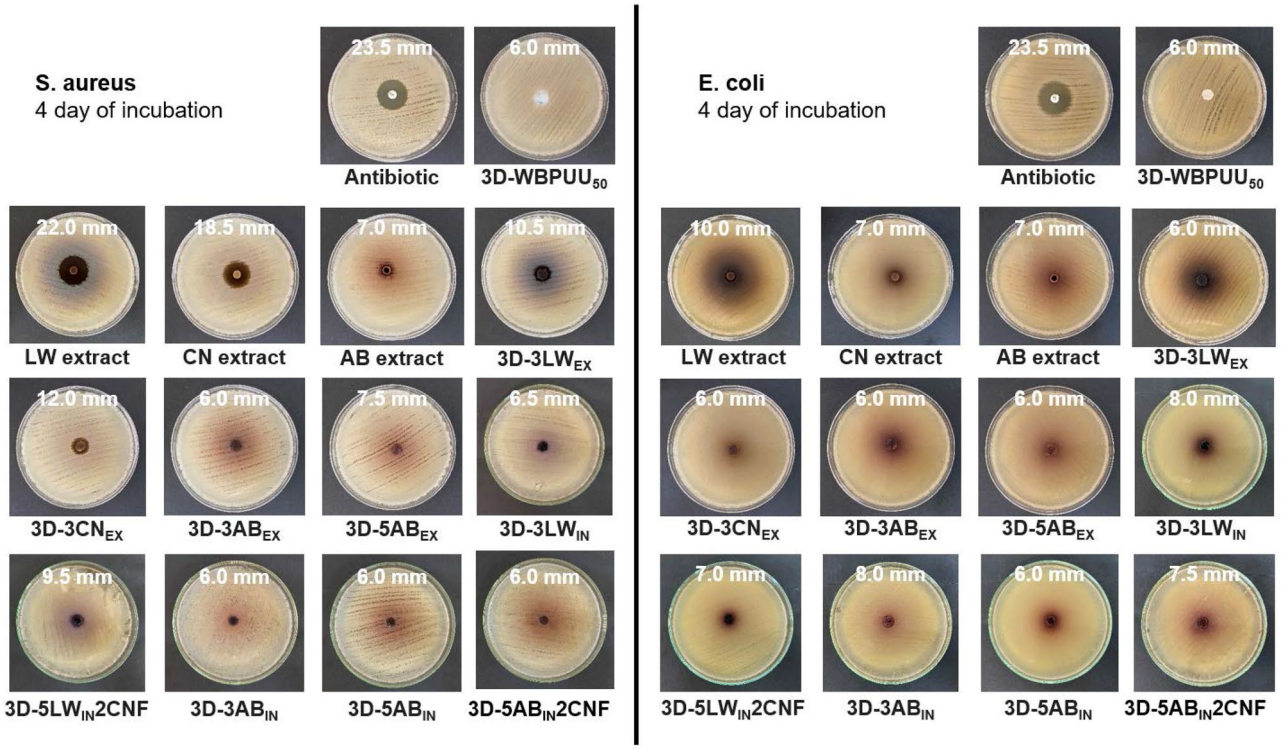

Fig. 12 Antibacterial tests for natural extracts and 3D printed parts against *S. aureus* and *E. coli* after 4 days of incubation at 37 °C

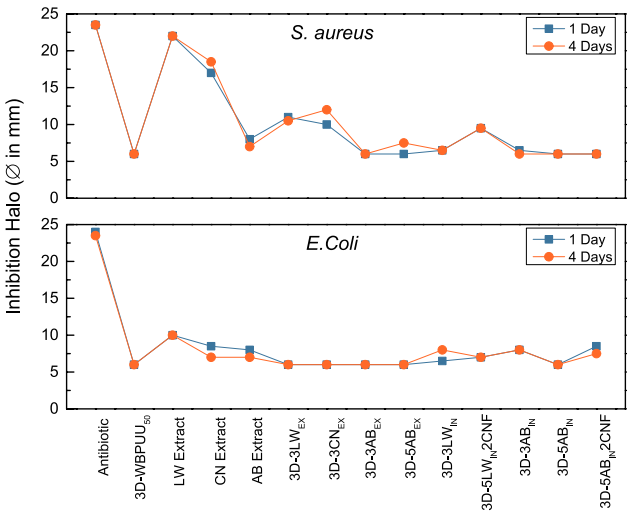

Fig. 13 Representation of the diameter of the inhibition halo against *S. aureus* and *E. coli*

strong bactericide capacity shown by logwood and chestnut extract containing composites is to be noted.

Overall, 5LWIN2CF ink presented the best behavior, showing the most successful printing process and the best final properties, both mechanical and antimicrobial. The good properties of the logwood extract, together with the highest homogeneity of the in-situ incorporation route and the addition of CNF, resulted on an ink with very promising capacities.

Supplementary Information The online version contains supplementary material available at https://doi.org/10.1007/s10924-023-03044-0.

Acknowledgements Financial support from the Basque Country Government in the frame of Grupos Consolidados (IT-1690-22) and Elkartek KK19-00048 is gratefully acknowledged. We also acknowledge the "Macrobehavior-Mesostructure-Nanotechnology" SGIker unit from the UPV/EHU for their technical support.

Author Contributions IA: Investigation, methodology, formal analysis, Writing—Original draft preparation; ASE: Conceptualization, investigation, Writing—Reviewing and editing; IF: Methodology, investigation; FB: Conceptualization, Writing—Reviewing and editing, supervision; AA: Conceptualization, Writing—Reviewing and editing, supervision; AE: Conceptualization, Writing—Reviewing and editing, supervision.

Funding Open Access funding provided thanks to the CRUE-CSIC agreement with Springer Nature. Financial support from the Basque Government (Grupos Consolidados (IT-1690-22), Elkartek (KK19-00048)) is acknowledged.

Data Availability The data presented in this study are available on request from the corresponding author.

Declarations

Competing Interests The authors declare no competing interests.

6. References

1. Prasad LK, Smyth H (2016) 3D Printing technologies for drug delivery: a review. Drug Dev Ind Pharm 42:1019–1031. https://doi.org/10.3109/03639045.2015.1120743
2. Li H, Tan YJ, Leong KF, Li L (2017) 3D bioprinting of highly thixotropic alginate/methylcellulose hydrogel with strong interface bonding. ACS Appl Mater Interfaces 9:20086–20097. https://doi.org/10.1021/acsami.7b04216
3. Markstedt K, Mantas A, Tournier I et al (2015) 3D bioprinting human chondrocytes with nanocellulose-alginate bioink for cartilage tissue engineering applications. Biomacromolecules 16:1489–1496. https://doi.org/10.1021/acs.biomac.5b00188
4. Yi HG, Choi YJ, Jung JW et al (2019) Three-dimensional printing of a patient-specific engineered nasal cartilage for augmentative rhinoplasty. J Tissue Eng 10:204173141882479. https://doi.org/10.1177/2041731418824797
5. Rouse JG, Van Dyke ME (2010) A review of keratin-based biomaterials for biomedical applications. Mater (Basel) 3:999–1014. https://doi.org/10.3390/ma3020999
6. Olmos-Juste R, Alonso-Lerma B, Pérez-Jiménez R et al (2021) 3D printed alginate-cellulose nanofibers based patches for local curcumin administration. Carbohydr Polym 264:118026. https://doi.org/10.1016/j.carbpol.2021.118026
7. Murphy SV, Atala A (2014) 3D bioprinting of tissues and organs. Nat Biotechnol 32:773–785. https://doi.org/10.1038/nbt.2958
8. Bandyopadhyay A, Bose S, Das S (2015) 3D printing of biomaterials. MRS Bull 40:108–114. https://doi.org/10.1557/mrs.2015.3
9. Vadillo J, Larraza I, Calvo-Correas T et al (2021) Design of a waterborne polyurethane–urea ink for direct ink writing 3D printing. Mater (Basel) 14:3287. https://doi.org/10.3390/ma14123287
10. Olmos-Juste R, Guaresti O, Calvo-Correas T et al (2021) Design of drug-loaded 3D printing biomaterial inks and tailor-made pharmaceutical forms for controlled release. Int J Pharm 609:121124. https://doi.org/10.1016/j.ijpharm.2021.121124
11. Vadillo J, Larraza I, Calvo-correas T, Gabilondo N (2022) Bioactive inks suitable for 3D printing based on waterborne polyurethane urea, cellulose nanocrystals and Salvia extract. React Funct Polym 175:105286. https://doi.org/10.1016/j.reactfunctpolym.2022.105286
12. Akindoyo JO, Beg MDH, Ghazali S et al (2016) Polyurethane types, synthesis and applications: a review. RSC Adv 6:114453–114482. https://doi.org/10.1039/C6RA14525F
13. Hsieh CT, Hsu S (2019) Double-network polyurethane-gelatin hydrogel with tunable modulus for high-resolution 3D bioprinting. ACS Appl Mater Interfaces 11:32746–32757. https://doi.org/10.1021/acsami.9b10784
14. Chen Q, Mangadlao JD, Wallat J et al (2017) 3D printing biocompatible polyurethane/poly(lactic acid)/graphene oxide nanocomposites: anisotropic properties. ACS Appl Mater Interfaces 9:4015–4023. https://doi.org/10.1021/acsami.6b11793
15. Larraza I, Vadillo J, Calvo-Correas T et al (2021) Cellulose and graphene based polyurethane nanocomposites for fdm 3d printing: filament properties and printability. Polym (Basel). https://doi.org/10.3390/polym13050839
16. Honarkar H (2018) Waterborne polyurethanes: a review. J Dispers Sci Technol 39:507–516. https://doi.org/10.1080/01932691.2017.1327818
17. Vadillo J, Larraza I, Calvo-Correas T et al (2021) Role of in situ added cellulose nanocrystals as rheological modulator of novel waterborne polyurethane urea for 3D-printing technology. Cellulose 28:4729–4744. https://doi.org/10.1007/s10570-021-03826-6
18. Larraza I, Vadillo J, Santamaria-Echart A et al (2020) The effect of the carboxylation degree on cellulose nanofibers and waterborne polyurethane/cellulose nanofiber nanocomposites properties. Polym Degrad Stab 173:109084. https://doi.org/10.1016/j.polymdegradstab.2020.109084
19. Hormaiztegui MEV, Daga B, Aranguren MI, Mucci V (2020) Bio-based waterborne polyurethanes reinforced with cellulose nanocrystals as coating films. Prog Org Coatings 144:105649. https://doi.org/10.1016/j.porgcoat.2020.105649
20. Chen R, De, Huang CF, Hsu S (2019) Composites of waterborne polyurethane and cellulose nanofibers for 3D printing and bioapplications. Carbohydr Polym 212:75–88. https://doi.org/10.1016/j.carbpol.2019.02.025
21. Wong CC, Li H, Bin, Cheng KW, Chen F (2006) A systematic survey of antioxidant activity of 30 chinese medicinal plants using the ferric reducing antioxidant power assay. Food Chem 97:705–711. https://doi.org/10.1016/j.foodchem.2005.05.049
22. Jaberian H, Piri K, Nazari J (2013) Phytochemical composition and in vitro antimicrobial and antioxidant activities of some medicinal plants. Food Chem 136:237–244. https://doi.org/10.1016/j.foodchem.2012.07.084
23. Stefanović O, Comic L (2012) Synergistic antibacterial interaction between Melissa officinalis extracts and antibiotics. J Appl Pharm Sci 2:1–5
24. Santamaria-Echart A, Fernandes I, Barreiro F et al (2018) Development of waterborne polyurethanepolyurethane–ureas added with plant extracts: study of different incorporation routes and their influence on particle size, thermal, mechanical and antibacterial properties. Prog Org Coatings 117:76–90. https://doi.org/10.1016/j.porgcoat.2018.01.006
25. Santamaria-Echart A (2017) Synthesis and characterization of waterborne polyurethane and polyurethane–urea towards ecofriendly materials by cellulose nanocrystals and plant extracts incorporation. University of the Basque Country
26. Đukanović S, Cvetković S, Lončarević B et al (2020) Antistaphylococcal and biofilm inhibitory activities of Frangula alnus bark ethyl-acetate extract. Ind Crops Prod. https://doi.org/10.1016/j.indcrop.2020.113013
27. Sadowska B, Paszkiewicz M, Podsędek A et al (2014) Vaccinium myrtillus leaves and Frangula alnus bark derived extracts as potential antistaphylococcal agents. Acta Biochim Pol 61:163–169. https://doi.org/10.18388/abp.2014_1939
28. Nejabatdoust A, Daemi HB, Salehzadeh A, Azimi SC (2020) Comparing of effects of hydro-alcoholic, ethanolic and methanolic extracts of the frangula alnus: chemical composition, antimicrobial and synergism. J Genet Resour 6:20–33. https://doi.org/10.22080/jgr.2020.2538
29. Wu CS, Liao HT (2014) The mechanical properties, biocompatibility and biodegradability of chestnut shell fibre and polyhydroxyalkanoate composites. Polym Degrad Stab 99:274–282. https://doi.org/10.1016/j.polymdegradstab.2013.10.019
30. Casillas PEG, Casillas PEG, Hernandez JL (2013) Biocompatibility of chitosan/Mimosa tenuiflora scaffolds for tissue engineering Related papers

31. Chiarini A, Micucci M, Malaguti M et al (2013) Sweet chestnut (*Castanea sativa* Mill.) bark extract: cardiovascular activity and myocyte protection against oxidative damage. Oxid Med Cell Longev. https://doi.org/10.1155/2013/471790
32. Vekiari SA, Gordon MH, García-Macías P, Labrinea H (2008) Extraction and determination of ellagic acid contentin chestnut bark and fruit. Food Chem 110:1007–1011. https://doi.org/10.1016/j.foodchem.2008.02.005
33. Kremer D, Kosalec I, Locatelli M et al (2012) Anthraquinone profiles, antioxidant and antimicrobial properties of *Frangula rupestris* (Scop.) Schur and *Frangula alnus* Mill. Bark. Food Chem 131:1174–1180. https://doi.org/10.1016/j.foodchem.2011.09.094
34. Ortiz-Hidalgo C, Pina-Oviedo S (2019) Hematoxylin: mesoamerica's gift to histopathology. Palo de Campeche (Logwood tree), pirates' most desired treasure, and irreplaceable tissue stain. Int J Surg Pathol 27:4–14. https://doi.org/10.1177/1066896918787652
35. Escobar-Ramos A, Lobato-García CE, Zamilpa A et al (2017) Homoisoflavonoids and chalcones isolated from *Haematoxylum campechianum* L., with spasmolytic activity. Molecules 22:1–10. https://doi.org/10.3390/molecules22091405
36. Han J, Chen TX, Branford-White CJ, Zhu LM (2009) Electrospun shikonin-loaded PCL/PTMC composite fiber mats with potential biomedical applications. Int J Pharm 382:215–221. https://doi.org/10.1016/j.ijpharm.2009.07.027
37. Venugopal JR, Sridhar S, Ramakrishna S (2014) Electrospun plant-derived natural biomaterials for tissue engineering. Plant Sci Today 1:151–154. https://doi.org/10.14719/pst.2014.1.3.65
38. Martel-Estrada SA, Rodríguez-Espinoza B, Santos-Rodríguez E et al (2015) Biocompatibility of chitosan/mimosa tenuiflora scaffolds for tissue engineering. J Alloys Compd 643:S119–S123. https://doi.org/10.1016/j.jallcom.2015.01.034
39. Yang Z, Peng H, Wang W, Liu T (2010) Crystallization behavior of poly(ε-caprolactone)/layered double hydroxide nanocomposites. J Appl Polym Sci 116:2658–2667. https://doi.org/10.1002/app
40. Zhu Z, Li R, Zhang C, Gong S (2018) Preparation and properties of high solid content and low viscositywaterborne polyurethane-acrylate emulsion with a reactive emulsifier. Polym (Basel). https://doi.org/10.3390/polym10020154
41. Cyriac F, Lugt PM, Bosman R (2015) On a new method to determine the yield stress in lubricating grease. Tribol Trans 58:1021–1030. https://doi.org/10.1080/10402004.2015.1035414
42. Hou J, Ma Y, Zhang Z et al (2019) The relationship between solid content and particle size ratio of waterborne polyurethane. Coatings 9:1–9. https://doi.org/10.3390/COATINGS9060401
43. Bao L, Fan H, Chen Y et al (2018) Synthesis of 1,4-butanediol di(3-diethylamino-2-hydroxylpropyl alcohol) ether and cationic waterborne polyurethane with high solids content. Adv Polym Technol 37:906–912. https://doi.org/10.1002/adv.21736
44. Wang C, Zhang J, Huang J et al (2021) Flame retardant modified bio-based waterborne polyurethane dispersions derived from castor oil and soy polyol. Eur J Lipid Sci Technol 123:1–7. https://doi.org/10.1002/ejlt.202000248
45. Peng SJ, Jin Y, Cheng XF et al (2015) A new method to synthesize high solid content waterborne polyurethanes by strict control of bimodal particle size distribution. Prog Org Coatings 86:1–10. https://doi.org/10.1016/j.porgcoat.2015.03.013
46. Díez-García I, Santamaría-Echart A, Eceiza A, Tercjak A (2018) Synthesis and characterization of environmentally-friendly waterborne poly(urethane-urea)s. Eur Polym J 99:240–249. https://doi.org/10.1016/j.eurpolymj.2017.12.026
47. Lee J, Kim M, Hong CK, Shim SE (2007) Measurement of the dispersion stability of pristine and surface-modified multiwalled carbon nanotubes in various nonpolar and polar solvents. Meas Sci Technol 18:3707–3712. https://doi.org/10.1088/0957-0233/18/12/005
48. Sharma T, Suresh Kumar G, Chon BH, Sangwai JS (2014) Viscosity of the oil-in-water Pickering emulsion stabilized by surfactant-polymer and nanoparticle-surfactant-polymer system. Korea Aust Rheol J 26:377–387. https://doi.org/10.1007/s13367-014-0043-z
49. Yang J, Pal R (2020) Investigation of surfactant-polymer interactions using rheology and surface tension measurements. Polym (Basel) 12:1–20. https://doi.org/10.3390/polym12102302
50. Jiang J, Oguzlu H, Jiang F (2021) 3D printing of lightweight, super-strong yet flexible all-cellulose structure. Chem Eng J 405:126668. https://doi.org/10.1016/j.cej.2020.126668
51. Ma T, Lv L, Ouyang C et al (2021) Rheological behavior and particle alignment of cellulose nanocrystal and its composite hydrogels during 3D printing. Carbohydr Polym 253:117217. https://doi.org/10.1016/j.carbpol.2020.117217
52. Liu S, Bao H, Li L (2016) Thermoreversible gelation and scaling laws for graphene oxide-filled κ-carrageenan hydrogels. Eur Polym J 79:150–162. https://doi.org/10.1016/j.eurpolymj.2016.04.027
53. Lin LG, Liu QY, Ye Y (2014) Naturally occurring homoisoflavonoids and their pharmacological activities. Planta Med 80:1053–1066. https://doi.org/10.1055/s-0034-1383026
54. Escobar-Ramos A, Lobato-García CE, Zamilpa A et al (2017) Homoisoflavonoids and chalcones isolated from *Haematoxylum campechianum* L., with spasmolytic activity. Molecules 22:2–11. https://doi.org/10.3390/molecules22091405
55. Lampire O, Milla I, Raminosoa M et al (1998) Polyphenols isolated from the bark of castanea. Phytochemistry 49:623–631
56. Gonçalves RS, Silva EL, Hioka N et al (2018) An optimized protocol for anthraquinones isolation from *Rhamnus frangula* L. Nat Prod Res 32:366–369. https://doi.org/10.1080/14786419.2017.1356836
57. Kar A (2012) Frangula-Buckthorn bark; Alder buckthorn; Black dogwood; Berry alder; Arrow wood; Persian berries. http://www.epharmacognosy.com/2012/03/frangula-buckthorn-bark-alder-buckthorn.html. Accessed 22 Jun 2021
58. Nasrollahzadeh M, Issaabadi Z, Sajadi SM (2018) Green synthesis of a Cu/MgO nanocomposite by: Cassytha filiformis L. extract and investigation of its catalytic activity in the reduction of methylene blue, congo red and nitro compounds in aqueous media. RSC Adv 8:3723–3735. https://doi.org/10.1039/c7ra13491f
59. Rafiee Z, Barzegar M, Sahari MA, Maherani B (2017) Nanoliposomal carriers for improvement the bioavailability of high-valued phenolic compounds of pistachio green hull extract. Food Chem 220:115–122. https://doi.org/10.1016/j.foodchem.2016.09.207
60. Shabbir M, Islam SU, Bukhari MN et al (2017) Application of Terminalia chebula natural dye on wool fiber: evaluation of color and fastness properties. Text Cloth Sustain. https://doi.org/10.1186/s40689-016-0011-8
61. Santamaria-Echart A, Fernandes I, Ugarte L et al (2021) Green nanocomposites from salvia-based waterborne polyurethane-urea dispersions reinforced with nanocellulose. Prog Org Coat 150:105989. https://doi.org/10.1016/j.porgcoat.2020.105989
62. Larraza I, Alonso-Lerma B, Gonzalez K et al (2020) Waterborne polyurethane and graphene/graphene oxide-based nanocomposites: reinforcement and electrical conductivity. Express Polym Lett 14:1018–1033. https://doi.org/10.3144/expresspolymlett.2020.83
63. Pershin GN, Malovanova SN, Kakeeva OO (1978) Antimicrobial activity of vinyloxyphenylazomethines. Russ Pharmacol Toxicol 41:175

64. Živković J, Zeković Z, Mujić I et al (2010) Scavenging capacity of superoxide radical and screening of antimicrobial activity of *Castanea sativa* mill. Extracts. Czech J Food Sci 28:61–68. https://doi.org/10.17221/155/2009-cjfs
65. Bacha A, Ben, Jemel I, Moubayed NMS, Abdelmalek I, Ben (2017) Purification and characterization of a newly serine protease inhibitor from *Rhamnus frangula* with potential for use as therapeutic drug. Biotech 7:1–13. https://doi.org/10.1007/s13205-017-0764-z
66. Yasunaka K, Abe F, Nagayama A et al (2005) Antibacterial activity of crude extracts from mexican medicinal plants and purified coumarins and xanthones. J Ethnopharmacol 97:293–299. https://doi.org/10.1016/j.jep.2004.11.014
67. Kleanthous C, Armitage JP (2015) The bacterial cell envelope. Philos Trans R Soc B Biol Sci 370:1–17. https://doi.org/10.1098/rstb.2015.0019
68. Zarayneh S, Sepahi AA, Jonoobi M, Rasouli H (2018) Comparative antibacterial effects of cellulose nanofiber, chitosan nanofiber, chitosan/cellulose combination and chitosan alone against bacterial contamination of iranian banknotes. Int J Biol Macromol 118:1045–1054. https://doi.org/10.1016/j.ijbiomac.2018.06.160